

Bachelor Project



**Czech
Technical
University
in Prague**

F3

**Faculty of Electrical Engineering
Department of Microelectronics**

Surface Characterisation of Diamond Structures

Rudolf Stanko

**Supervisor: doc. RNDr. Jan Voves, CSc.
October 2022**

Acknowledgements

I would like to thank docent Jan Voves for this opportunity to work on such amazing project. For his helping hand in every aspect and professional guidance throughout whole time I have spent on this thesis. Furthermore I would like to thank my brothers for being supportive and willing to discuss any questions regarding my struggles with writing.

Declaration

I declare that this work is all my own work and I have cited all sources I have used in the bibliography in accordance with the Methodical instructions that cover the ethical principles for writing an academic thesis.

Prague, October 22, 2022

Prehlasujem, že som predloženú prácu vypracoval samostatne, a že som uviedol všetkú použité informačné zdroje v súlade s Metodickým pokynom o dodržovaní etických princípov pri príprave vysokoškolských záverečných prác.

V Prahe, októbra 22, 2022

Abstract

This thesis will introduce the reader to the basics of synthetic diamonds. Different types of preparation will be briefly explained, and readers will be introduced to the basic types of diamonds based on their properties. Later, we will look at some properties closely related to use in the electrical industry for semiconductor devices. At the end of the theoretical part, two methods for sample characterisation are described, atomic force microscopy and Raman spectroscopy. In the experimental part, a closer look at four samples is made. Each sample has a different surface orientation on the homo-epitaxial boron-doped diamond in order: (100), (111), (113) and (115). On each, AFM scans are done, and Raman spectra taken, followed by a discussion of results and comparing them to knowledge about these surfaces from different studies.

Keywords: atomic force microscopy, Raman spectroscopy, semiconductors, synthetic diamonds

Supervisor: doc. RNDr. Jan Voves, CSc.
Faculty of Electrical Engineering,
Czech Technical University in Prague,
Technická 2,
Praha 6

Abstrakt

Táto práca uvedie čitateľa do základov o syntetických diamantoch. Stručne vysvetlí rôzne typy výroby a typy diamantov v závislosti od ich vlastností. Neskôr sa pozrie na vlastnosti úzko späté s použitím v elektrotechnickom priemysle pri výrobe polovodičkových súčiastok. Na konci teoretickej časti sa dozvie niečo o dvoch metódach určovania charakteristík vzorkov pomocou mikroskopie atomárnych síl a Ramanovej spektroskopie. V experimentálnej časti sú uvedené štyri vzorky s rôznymi orientáciami povrchov v poradí (100), (111), (113) a (115). Na každej vzorke je prevedený scan povrchu pomocou AFM a určené Ramanovo spektrum. Tieto vlastnosti sú potom porovnané s výsledkami z rôznych štúdií.

Kľúčové slová: mikroskopia atomárnych síl, Ramanova spektroskopie, polovodiče, syntetické diamanty

Preklad názvu: Charakterizácia povrchov diamantových štruktúr

Contents

1 Introduction	1
2 Diamond Structures	5
2.1 Carrier mobility	5
2.2 Saturation velocity and carrier lifetime	6
2.3 Dielectric breakdown field and wide bandgap	7
2.4 Thermal conductivity	7
2.5 Diamond device applications	9
2.6 Challenges of working with diamond	12
3 Atomic Force Microscopy	15
3.1 Basics and principles	15
3.2 Other capabilities of AFM	19
4 Raman Spectroscopy	21
4.1 Basics and principles	21
4.2 Other capabilities of Raman spectroscopy	23
5 Experimental Part	27
5.1 Theoretical introduction	27
5.2 Sample properties	29
5.2.1 (100) oriented homo-epitaxial boron-doped diamond	29
5.2.2 (111) oriented homo-epitaxial boron-doped diamond	32
5.2.3 (113) oriented homo-epitaxial boron-doped diamond	34
5.2.4 (115) oriented homo-epitaxial boron-doped diamond	37
6 Conclusion	39
Bibliography	41

Figures

<p>1.1 Different diamonds, based on how they grew and their growth morphology [1] 3</p> <p>1.2 Table of different diamond gems' colours based on their types [2] 4</p> <p>2.1 Structures of different Unipolar and Bipolar diodes[3] 10</p> <p>2.2 (a)Enlargement of the area during the crystal growth in cases of Si and SiC (left) and Shrinking of the area during crystal growth in case of SCD due to gas containing nitrogen (right) (b)three-dimensional growth of SCD 13</p> <p>2.3 Diamond wafer using different mosaic techniques 14</p> <p>3.1 Force response curve of the tip [4] 16</p> <p>3.2 Force displacement curve [5].... 17</p> <p>4.1 Principle of Raman scattering [6] 21</p> <p>4.2 Illustration of SERS principle [7] 24</p> <p>5.1 AFM microscope from NTEGRA [8] 28</p> <p>5.2 Raman spectroscopy microscope from Renishaw [9] 28</p> <p>5.3 Close look at the (100) sample under build-in optical microscope in Raman spectroscopy with highlighted area of scan (8x8 μm) 29</p> <p>5.4 AFM scan of highlighted area with next, more detailed scan of what appeared to be narrow surface 30</p> <p>5.5 Raman scan of the sample at random selected point 30</p> <p>5.6 Height profile comparison of one going pass by the L-shaped structure and one going through it..... 31</p> <p>5.7 Close look at the (111) sample under build-in optical microscope in Raman spectroscopy with highlighted area of scan 32</p> <p>5.8 Comparison of differences between uncorrected (left) and corrected (right) slope of the scan on AFM sample 33</p>	<p>5.9 Height profile of selected line at (111) orientation 33</p> <p>5.10 Raman spectra of randomly selected point in the scanning area of the (111) sample..... 34</p> <p>5.11 Close look at the (113) sample under build-in optical microscope in Raman spectroscopy with highlighted area of scan 34</p> <p>5.12 Height profile with shown lines on AFM scan of the sample 35</p> <p>5.13 3D profile of scanned area (2.2x2.2 μm) 35</p> <p>5.14 Raman spectra of (113)-oriented homo-epitaxial boron-doped diamond with no sign of fluorescence 36</p> <p>5.15 Close look at the (115) sample under build-in optical microscope in Raman spectroscopy with highlighted area of scan 37</p> <p>5.16 AFM scan of larger area 12x12 μm and then detailed scan of partly-selected area of 2x2 μm.... 37</p> <p>5.17 Comparison of height profiles with shown lines on AFM scans... 38</p> <p>5.18 Raman spectra of (115) oriented homo-epitaxial boron-doped diamond 38</p>
--	--

Tables

2.1 Comparison of material properties materials mostly used in semiconductor industry	8
2.2 Comparison of materials given by different Figures of Merit, normalized to $\text{Si} = 1$ at room temperature [10].	9
2.3 Summary of diamond diodes. Performance variables listed are not obtained from the same device, but are the best values for each diode separately reported to date [3]	10



Chapter 1

Introduction

Surprisingly, diamonds share some common characteristics with coal. Both are composed of the most common substance on earth: carbon. This was discovered in 1797. What makes diamonds different from coal is how the carbon atoms are arranged and how the carbon is formed. Diamond molecules are stacked neatly into uniform lattices, which is why they are so hard and crystal clear. Coal molecules, by comparison, are randomly stacked, which gives coal its colour and the fact that it burns and can easily be broken into smaller pieces.

Natural diamonds were formed more than 1 billion years in depths between 150 and 250 kilometres in the earth's mantle under high pressures and temperatures. These conditions allowed carbon-containing fluids around minerals to form diamonds. They are very rare to occur in nature and tough to find. About 250 tons of earth must be moved to find a single carat of diamond [11]. Diamonds have been adopted for many uses because of the material's exceptional physical characteristics. It has the highest thermal conductivity and the highest sound velocity. It has low adhesion and friction, and its coefficient of thermal expansion is extremely low. Its optical transparency extends from the far infrared to the deep ultraviolet and has high optical dispersion. It also has high electrical resistance. It is chemically inert, not reacting with most corrosive substances, and has excellent biological compatibility. Pure diamond is also an electrical insulator, but with impurities such as nitrogen or boron within, it becomes a conductor.

Because of its rarity, techniques have been developed to create artificial diamonds called synthetic. First attempts were made even at the end of the 19th century but were not confirmed, thus not recognised as actual research. In the 1940s, systematic research on diamond creation began in the United States, Sweden and the Soviet Union. The first synthesis was made in 1954 in Stockholm by GE (General Electric) under a project codename **Project Superpressure**. This diamond was made by pressure above 10 *GPa* and temperature over 2 000°C. Although the created diamond was only 0.15 *mm* across and visually imperfect for jewellery, it was usable in industry. The whole process was well-documented and verifiable [12, 13].

Nowadays, to produce synthetic diamonds, two major methods are used. One uses high pressure and high temperature and thus is called high-pressure high-temperature (HPHT). Typical growth conditions are from 1 400°C to 1 600°C and from 50 to 60 kbar. Under these, the diamond is in the stable phase of carbon. A small sample of a diamond called the seed is then placed into a chamber along with some source of carbon. Commonly used is graphite. There is also needed a catalyst to speed up the reaction. Typically used are iron, nickel or manganese. It takes at least five days to grow 1 – ct of diamond, which corresponds to 0.2 g [14].

The second one creates a carbon plasma over a substrate onto which carbon atoms are deposited to form a diamond structure. This is called chemical vapour deposition (CVD). This method is very similar to the natural process of creating diamonds. A thin layer is cut from the natural diamond to form the CVD diamond seed. Primarily Type IIa is used (different types of diamonds are discussed later in this thesis). It is polished and prepared to the required thickness to be then placed in a CVD plasma reactor. At a temperature of about 800°C and pressure under 27kPa, the seed is exposed to a mixture of methane gas and hydrogen in a ratio 1 : 99. They are then together exposed to microwaves to break them up into plasma. Inside the plasma, hydrogen atoms bash into hydrogen molecules and into methane molecules to create carbon-growth species. The hydrogen also covers the surface to stop it from forming graphite. Every now and then, the hydrogen is removed from the surface, and carbon-growth species attach, building up the diamond. This cycles and thus grows the diamond layer by layer [15]. Naturally, other methods exist, such as detonating explosives or ultrasound cavitation.

We can classify diamonds into five types based on how many chemical impurities and what types there are. Different diamond types can coexist within a single stone and react differently to enhancement techniques. Impurities are measured at the atomic level and are expressed in ppm, which states for **parts per million**. It says how many atoms are in a lattice per million of pure material. Since these impurities are at the atomic scale, infrared spectrometer is commonly used for detection.

The first type is Type I. This is the most common class, containing nitrogen as the main impurity. Based on the concentration of impurities, there are two sub-types, Type Ia and Type Ib. Type I diamonds have a characteristic fluorescence effect and visible absorption spectrum. They also absorb in both infrared and ultraviolet regions.

In Type Ia, the nitrogen impurities make up to 0.3%, corresponding to 3 000ppm, clustered within the carbon lattice and relatively widespread. If the nitrogen atoms are in pairs, they are determined as Type IaA, if they


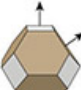
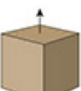
Growth Process	Typical Growth Morphology
Natural	 <p>Shape: Octahedron Growth: 8 directions</p>
High Pressure, High Temperature (HPHT)	 <p>Shape: Cuboctahedron Growth: 14 directions</p>
Chemical Vapor Deposition (CVD)	 <p>Shape: Cube Growth: 1 direction</p>

Figure 1.1: Different diamonds, based on how they grew and their growth morphology [1]

are in large even-numbered aggregates, they are called Type IaB. Most Type Ia diamonds contain a mixture of both of these categories. These make up about 95% of all natural diamonds.

In Type Ib, diamonds contain up to 0.05% of nitrogen impurities, which is about 500ppm, but they are more diffused and dispersed throughout crystal in isolated sites. These make up about 0.1% of all natural diamonds.

Type II diamonds have no measurable nitrogen impurities. These absorb in a different infrared spectrum region and transmit in the ultraviolet. In nature, they are larger than Type I and tend to have more irregular shapes. They were formed under extremely high pressure for more extended time periods.

Type IIa diamonds make up to 1 – 2% of all natural diamonds. They rarely contain any impurities and can easily be repaired by a high-pressure, high-temperature process. This process will also remove the diamond's colour since they are the leading cause of colouring in diamonds.

Type IIb diamonds are the rarest, hence very valuable. They make up only 0.1% of all natural diamonds. They, too, contain very few nitrogen impurities comparable to Type IIa but have significant boron impurities. These are the most suitable to be used for semiconductors. Since boron has three valence electrons and diamond, which is made out of carbon, has four, boron acts as an acceptor and thus can together create a p-type semiconductor. For this effect, as little as one ppm of boron is enough to have a visible impact.

It is also possible to pre-determine diamond types by different colours. Type Ia tends to be pale yellow or light brown since nitrogen absorbs blue light. They also show blue fluorescence to long-wave UV radiation. Type

Ib diamonds absorb green light in addition to blue and thus have darker colours, appearing in darker brown and yellow. All Type II diamonds are much clearer and transparent, but the anomalies in structural deformation or some impurities give them sparks of colour. They can differ, and we can see even orange, pink, red or purple gems in nature. For Type IIb there are most common to be light blue or grey. Boron impurities mainly cause this [2, 16, 17].

Type	Colors of Natural Diamonds	Colors of Treated Natural Diamonds	Colors of Synthetic and Treated Synthetic Diamonds
Ia			
Ib			
IIa			
IIb			

Figure 1.2: Table of different diamond gems' colours based on their types [2]

The never-ending demand for more capable materials has brought the idea of considering diamond as the new essential element for the semiconductor industry. Later in this thesis, the reader will be introduced to the basic properties of diamond structures, mainly concentrating on relevance to electronic applications and some features which present challenges in global production.

Chapter 2

Diamond Structures

Diamond is one of the most exceptional naturally occurring material, endowed with many extreme physical properties that enable a broad range of applications, particularly when combined. Aside from the fact that diamond is the hardest of all materials, which has led to its exploitation in a broad range of mechanical applications, its optical properties (including transmission across the ultraviolet to microwave wavelength range), in combination with its high thermal conductivity and low coefficient of thermal expansion make it a superb material. Unfortunately, these unique properties are rarely present all in the same stone. This puts natural diamonds aside from practical research and industrial use. Thus synthetic diamonds created by HPHT and CVD are used in numerous engineering applications. Thanks to the everlasting development of these techniques and ongoing research, it is now possible to specify some particular properties and further improve them depending on the demands for use. Such applications currently include precision optical components for high-power lasers, detector material for high-energy physics, heat spreaders for the telecommunication industry, and high-power generators or inverters for trains and ships.

2.1 Carrier mobility

Single-crystal diamond exhibits both the highest electron mobility and hole mobility as well among candidates for semiconductors. With electron mobility around $4\,500\text{ cm}^2\text{V}^{-1}\text{s}^{-1}$ and hole around $3\,800\text{ cm}^2\text{V}^{-1}\text{s}^{-1}$ in intrinsic single/crystal synthetic diamond at room temperature. Corresponding values for 4H-SiC are $900\text{ cm}^2\text{V}^{-1}\text{s}^{-1}$ for electrons and $120\text{ cm}^2\text{V}^{-1}\text{s}^{-1}$ for holes and $440\text{ cm}^2\text{V}^{-1}\text{s}^{-1}$ and $200\text{ cm}^2\text{V}^{-1}\text{s}^{-1}$ for GaN. When samples have been heated up to between 300-400 K, a drop in mobility as $T^{-1.5}$ has been observed. This is generally considered to be indicative of acoustic phonon scattering in high crystallographic quality, intrinsic samples as assessed by Isberg et al. [18]. However, Somogyi [19] points out that this reduction could also result from scattering from incomplete ionisation of common impurities within the diamond material. When the samples were heated over 400 K, hole mobility fell even more rapidly with an exponent reaching -2.5 and later even -3.66 . With this reduction, electron mobility at 500 K was measured to

be over $2\,000\text{ cm}^2\text{V}^{-1}\text{s}^{-1}$ and hole mobility over $1\,000\text{ cm}^2\text{V}^{-1}\text{s}^{-1}$ making high-temperature device operation still possible with leading numbers. The scattering of impurities throughout the sample causes mobility drop with increasing dopant concentration. Fox et al. [20] have measured hole mobility dropping from around $1500\text{ cm}^2\text{V}^{-1}\text{s}^{-1}$ to $1\,000\text{ cm}^2\text{V}^{-1}\text{s}^{-1}$ in B-doped CVD samples with B concentrations in the range $5.10^{16} - 2.10^{18}\text{ cm}^{-3}$. Element Six have shown in their unpublished data a few samples with hole Hall mobility of $450\text{ cm}^2\text{V}^{-1}\text{s}^{-1}$ for a B concentration of around $1\,019\text{ cm}^{-3}$. This means that even highly B-doped diamonds can exhibit pretty decent hole mobility. In devices, the active region should consist purely of the intrinsic diamond. Thus the drop in mobility with dopant concentration is not relevant. The next challenge is to achieve impurity-free material [21, 16].

2.2 Saturation velocity and carrier lifetime

In high electric fields, the conductivity is determined by the saturation velocity. The velocity of charge carriers is saturated at high fields by generating optical phonons in the crystal lattice. A high saturation velocity is advantageous for performing FETs operating at high frequencies. It is given by the equation:

$$V_s = \sqrt{\frac{8E_{opt}}{3\pi m^*} \tanh(E_{opt})/2kT} \quad (2.1)$$

where E_{opt} is the energy of optical phonons and m^* is the effective mass of the charge carriers. High optical phonon energies tend to give a high saturation carrier velocity. Diamond has the highest optical phonon energy among any semiconductor. Experimentally determined values of saturation velocity may vary in different works of literature because of different samples, but they mostly incline to intervals between $0.85 - 1.12 \cdot 10^7\text{ cm s}^{-1}$ for holes and $1.5 - 1.7 \cdot 10^7\text{ cm s}^{-1}$ for electrons.

Of the other wide-bandgap semiconductors, only SiC reaches values comparable to diamond ones. However, diamond has an absolute advantage in that its saturation velocity is reached in fields of approximately 10 kV/cm , whereas for SiC, the velocity saturates at fields close to its practical electrical breakdown strength. Such high fields can be challenging to approach in devices.

While designing bipolar components, carrier lifetime is crucial. It is equally important for devices where electron-hole pairs are generated by radiation, such as radiation detectors. For unipolar devices, the recombination lifetime is of less interest. However, a high carrier lifetime indicates a low impurity and defect concentration and thus can be used as an indicator of material quality. In single-crystal CVD-produced diamonds, a carrier lifetime of more than $2\mu\text{s}$ has been measured. This is quite similar to the one of 4H-SiC [21].

2.3 Dielectric breakdown field and wide bandgap

While designing power devices such as diodes and switches, which are intended to block several kilovolts or high-frequency FETs, we want a semiconductor material with a high electric breakdown field. The reason is that if higher electric fields can be tolerated, the design can push dimensions into smaller numbers, resulting in faster switching. Intrinsic breakdown in semiconductors is inherent to the material. It results from impact ionisation and subsequent avalanche breakdown. On the other hand, extrinsic breakdown at defects is dependent on the crystalline quality and improves with better quality material. Diamond presents the highest breakdown field (E_{br}) of any semiconductor with values in the range $5 - 10 \text{ MVcm}^{-1}$. In comparison, 4H-SiC has measured field at 3 MVcm^{-1} and GaN at around 5 MVcm^{-1} [21]. For extremely high voltage applications over 10 kV, wide bandgap bipolar devices are expected to open up a new opportunity in the future [14]. Diamond bipolar devices are a hopeful candidate owing to their favourable characteristics [21, 22].

2.4 Thermal conductivity

Diamond also has the highest thermal conductivity (T_c) among any known materials. The strong covalent bonding and low phonon scattering mostly cause this. Single-crystal CVD-produced diamond can have more than $2\,200 \text{ Wm}^{-1}\text{K}^{-1}$ at room temperature. This can drop to around $700 \text{ Wm}^{-1}\text{K}^{-1}$ at 770 K. The extremely high thermal conductivity of diamond enables diamond-based devices to handle high powers more simply. This is because the first stage of thermal management, which is getting any heat away from the point at which it is produced, is facilitated by the device itself rather than by an add-on solution. In the technological industry, it is used for efficient heat removal in high-end power electronics [21]. A diamond that uses deep energy level carriers has increased numbers at high temperatures. The trade-off in carrier increases with the mobility decrease brought by carrier scattering, resulting in a constant current between 150 and 250°C . This characteristic has inspired a new type of high output power device module operating at self-heating temperatures, which are thermally insulated without cooling [21, 22, 16].

	Si	4H-SiC	GaN	Natural diamond	Synthetic diamond	Potential device application benefit
Band gap (eV)	1.1	3.2	3.44	5.47	5.47	high temperature
Breakdown field (MV/cm^{-1})	0.3	3	5	10	10-20	high voltage
Hole mobility (cm^2/Vs)	480	120	200	1800-2100	3800	
Electron mobility (cm^2/Vs)	1,450	900	440	200-2800	4500	
Thermal conductivity ($Wcm^{-1}K^{-1}$)	1.5	5	1.5 - 3	22	24	high power
Hole saturation velocity($.10^7cms^{-1}$)	n/a	n/a	n/a	0.8	0.8	
Electron saturation velocity($.10^7cms^{-1}$)	0.86	3	2.5	2	2	high frequency

Table 2.1: Comparison of material properties materials mostly used in semiconductor industry

Since power electronics constantly evolve, standardisation protocols can only sometimes keep up with innovations. In order to distinguish better and worse power devices, it is necessary to create new data-based metrics for performance relative to its alternatives. One frequently used method is known as **Figures of Merit** (FoM)

$$JFOM = \frac{E_B^2 \cdot v_s^2}{4\pi^2} \quad (2.2)$$

Johnson FoM defines the power-frequency product for a low-voltage transistors. Here E_B is the critical electric field for breakdown in the semiconductor and v_s is the electron saturation velocity.

$$KFOM = \kappa \cdot \sqrt{\frac{c \cdot v_s}{4\pi\epsilon_s}} \quad (2.3)$$

Keyes FoM provides a thermal limitation to the switching behavior of transistors used in integrated circuits. Where κ is the thermal conductivity, c is velocity of light and ϵ_s is the static dielectric constant

$$BFOM = \varepsilon_s \cdot \mu \cdot E_g^3 \quad (2.4)$$

Baliga derived a figure of merit, which defines material parameters to minimize the conduction loss in low-frequency unipolar transistors. Here, μ is the mobility and E_g is the bandgap of the semiconductor.

	Si	4H-SiC	GaN	Diamond	
Johnson's FoM	1	410	280	8200	Power-frequency product
Keyes' FoM	1	5.1	1.8	32	Transistor behavior thermal limit
Baliga's FoM	1	290	910	17 200	Unipolar high-frequency device performance

Table 2.2: Comparison of materials given by different Figures of Merit, normalized to Si = 1 at room temperature [10]

2.5 Diamond device applications

Power semiconductor devices have been doubling in efficiency every three years for the last 18 years. The goal is simple and straight. To make power semiconductor devices faster, smaller, lighter, more reliable and with overall cost reduction. In many cases, systems have been optimised within the constraints of Si technology. However, the intrinsic properties of diamonds make it possible to satisfy the needs of the growing market beyond the scope of Si technology. The ideal power semiconductor device combines zero conduction losses with zero switching losses, thus maximising the efficiency of power electronics systems. Si unipolar power devices, such as the metal-oxide-semiconductor FET (MOSFET) or Schottky diode, offer near-ideal switching characteristics because of an absence of stored charge. However, conduction losses limit the maximum voltage rating of Si Schottky diodes to just 250 V, while Si MOSFETs are rarely used above 600 V. At higher voltages, bipolar devices are used; there is just one issue. Charge injection gives low conduction losses but at the cost of switching losses. Thus bipolar devices are essentially a balancing between these two parameters being adjusted to the needs of particular use. This can change with wide-bandgap materials. Material properties of CVD diamond offer higher critical electric fields, thermal conductivity and carrier mobility. This equates to higher power densities and higher efficiency systems. Progress in epitaxial growth and fabrication techniques, such as p- and n-type doping control with low compensation and surface treatment, have improved the performance of power devices.

One of the first diamond-based power devices to be reportedly made was a high-temperature diode. The large controllability of the Schottky

barrier height (SBH) for a diamond is one of its essential advantages. The operating temperature of a Schottky diode structure was pushed to over $1\,000^{\circ}\text{C}$. Its structure consisted of Si-based Schottky material deposited onto a homoepitaxial B-doped diamond surface [23]. This work was carried out under the Carbon Power Electronics (CAPE) consortium project and resulted in the fabrication of various Schottky barrier diodes (SBD) from single-crystal CVD diamonds. Brezeanu and co-workers [24] have revealed details of a metal-insulator-p-type (MIP) semiconductor diode structure. The MIP SBD structure can compensate for the lack of carriers in the drift region thanks to the high hole mobility in the intrinsic diamond. It can also withstand breakdown voltages of a few kilovolts with thin drift regions, which are less than $25\ \mu\text{m}$. This is a result of the high critical field strength of diamond structures. Ongoing careful design and research suggest that diamonds could become an important component in power conversion devices, capable of operating at voltages exceeding orders of 10 kVs and higher temperatures than any other semiconductor materials. In terms of diodes, both unipolar and bipolar, such as p-type-intrinsic-n-type diodes (PiNDs), SBDs, junction barrier Schottky diodes (JBSDs), metal-intrinsic-p type diodes (MiPDs), and Schottky pn diodes (SPNDs) have been experimentally reported in past few years [25, 3].

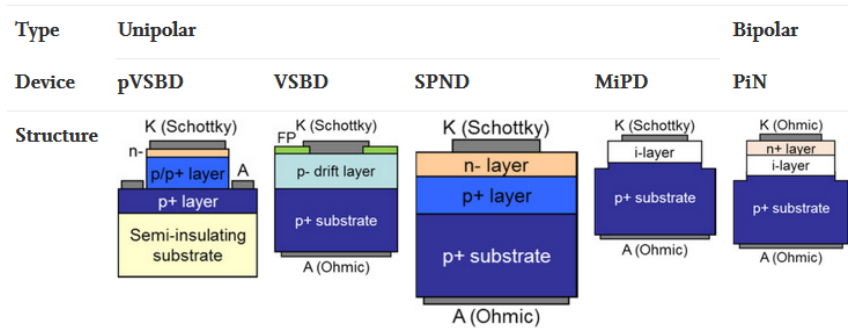


Figure 2.1: Structures of different Unipolar and Bipolar diodes[3]

Device	pVSBD	VSBD	SPND	MiPD	PiN
V_{max}	2.5 kV	1.8 kV	$>100\ \text{V}$	2.5 kV	$>10\ \text{kV}$
E_{max}	$> 7\ \text{MV/cm}$	$2.7\ \text{MV/cm}$	$3.4\ \text{MV/cm}$	$4.2\ \text{MV/cm}$	$3.4\ \text{MV/cm}$
I_{max}	0.5 A	20 A	$<100\ \text{mA}$	$<100\ \text{mA}$	$<100\ \text{mA}$
J_{max}	$> 4.5\ \text{kA/cm}^2$	$> 1\ \text{kA/cm}^2$	$> 60\ \text{kA/cm}^2$	$> 7.5\ \text{kA/cm}^2$	n/a
Challenges		Current capability	Defects	Low n-doping with low compensation	High current capability and High n+ doping

Table 2.3: Summary of diamond diodes. Performance variables listed are not obtained from the same device, but are the best values for each diode separately reported to date [3]

The electrical characteristics of diamonds permit the design of high-power switches with very low dynamic losses. Research in this segment started in the 1980s using natural diamonds. The first to be realised was the bipolar junction transistor (BJT). Natural p-type diamond crystal was used as a base electrode with an n-type emitter and collector regions made of carbon ion implantation. Shortly after, it was followed by attempts to create metal-semiconductor FETs (MESFETs) and metal-insulator-semiconductor FETs (MISFETs) also on natural diamond crystals.

It should be possible to make 1.7 kV and 6.5 kV switches that operate at several kilohertz with stable currents. Switching losses are also reduced from the current 3% to less than 1%. This can dramatically reduce losses caused by harmonics in physical structures. In addition, the excellent thermal characteristics of diamonds permit the manufacture of devices to operate up to 400°C. An active cooling system will no longer be needed thanks to excellent thermal conductivity, improving the overall system efficiency. Lastly, the allowable current density will be far higher than in Si devices, and the required semiconductor area will be dramatically reduced.

In terms of power devices, a desirable goal is to produce an efficient 20 kV switch (FET and/or radiation-activated switch) capable of replacing thyristors and IGBTs (Insulated Gate Bipolar Transistor), which are currently primarily used. For example, in high-voltage, direct-current (HVDC) and traction applications. Diamond is now being considered a serious contender in this area. It is currently standard for high-power FETs to build them vertically. This is to ensure a large cross-section for the current flow. This type of device's manufacturing process requires highly complex processing steps like deep-trench etching. Methods suitable for mass volume production are still in development [21, 24, 26].

The figures of merit for diamond as a device material have resulted in considerable efforts aimed at transistor designs by groups worldwide. The performance of diamond devices has been improved since the establishment of homoepitaxial growth techniques and doping control. However, the lack of device fabrication techniques still limits device performance. New processing techniques to form edge-termination structures, especially on selectively doped substrates using ion implantation or selective area growth, together with MOS structures, are required for effective use of the attractive properties of diamond. A deeper understanding of surface, interface, and defect structures are necessary to improve device fabrication, and performance [21, 24, 26].

2.6 Challenges of working with diamond

While all of the above-presented characteristics are overwhelming, there are several challenges in the applications of diamond structures. The realisation of the significant potential of diamond devices over existing device technology depends on completing several key objectives.

- access in volume to high-quality, high-purity material
- the capability of providing carriers by doping the material in a controlled manner
- the ability to process thin layers and structures

Single-crystal CVD diamond plates are currently available and are suitable for the electronic industry. They are commonly used in the fabrication of Schottky diodes and FETs.

Concerning the second objective for realising diamond devices, i.e. the capability of providing carriers by doping the material in a controlled manner, a considerable amount of effort has gone into the search for suitable dopants. Dopants in wide-bandgap semiconductors tend to have higher ionisation energies than those in narrow-bandgap semiconductors, resulting in low activation at room temperature. In the case of a diamond, known dopants have even higher ionisation energies. The most used diamond dopants are boron for p-type and nitrogen or phosphorus for n-type [27, 21]. However, as B acceptors are only weakly activated at room temperature (because ionisation energy is 0.37 eV), considerable effort has been focused on research into novel unipolar designs based on B doping to realise functional semiconductor devices in CVD diamond.

Lastly, the ability to process nanoscale layers and structures is the final but most challenging aspect of creating active electronic components. Nowadays, commercially available SCD is much smaller than other semiconductor materials. Si available as 300 mm wafers and SiC in 100-150 mm. Diamond wafers are typically available in sizes around 1 cm^2 or smaller. Several reasons limit the production of larger wafers, and they can be distributed into three parts [28].

Firstly, it isn't easy to grow SCD over a larger area and maintain sufficient crystal quality simultaneously. High-quality SCD can be fabricated using the HPHT method, but they cannot be produced in desired dimensions and growth rate. CVD is more promising in this area and generally has no strict limits to the deposition area. The only true limitation is dependence is the size of the seed crystal. This way, we conclude the second problem: the size of the seed itself. For both Si and SiC, the area of the growing block can be enlarged during growth. However, the area of SCD tends to shrink during the process, especially when nitrogen is present. Figure 2.2.

This can be reduced by making them grow in a specified direction. For example, small amounts of nitrogen are introduced into the system to enhance

the growth rate of the 100 direction and suppress the growth of abnormal directions at the substrate's top surface. This improves the repeatability of the growth but does not enlarge the area of the substrate as shown in Figure 2.2 too. This experiment was done by Mokuno et al. [29]. It is not easy to maintain such a sensitive parameter for extended periods. After the growth of SCD on the (100) face, the (010) side was polished and an additional layers of SCD were deposited on the surface. Repeating this process resulted in an enlarged seed of half-inch size. Even at the growth rate of several $10 \mu\text{m}/\text{h}$, it takes more than 1 000 hours to enlarge a half-inch SCD seed into 1-inch plate.

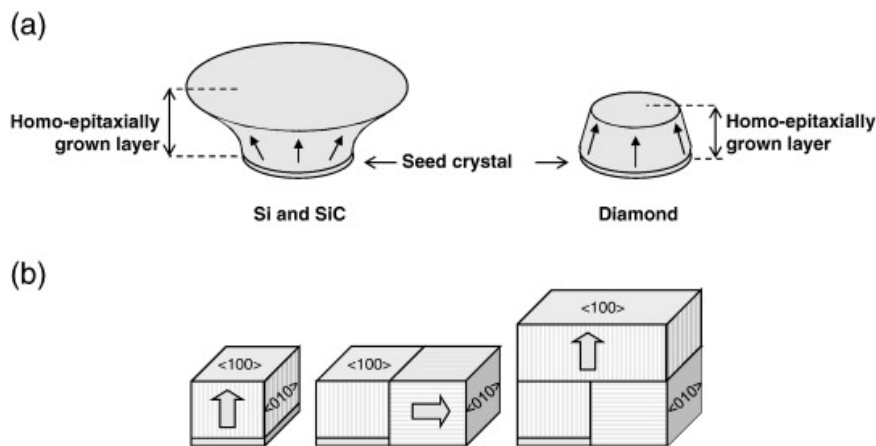


Figure 2.2: (a) Enlargement of the area during the crystal growth in cases of Si and SiC (left) and Shrinking of the area during crystal growth in case of SCD due to gas containing nitrogen (right)
(b) three-dimensional growth of SCD

The third problem is that of producing actual electron devices onto SCD plates. Therefore, another method was studied for fabricating large wafers using a so-called mosaic wafer. SCD layers are grown on relatively small plates of SCD, which have been arranged appropriately so that the upper layer joins the smaller plates into one larger wafer. Suppose the smaller SCD plates are more significant than the device size. In that case, this method may be practical for producing electronic devices and realise the inch-sized wafer within an acceptable time. The maximum size of the mosaic wafer obtained by this method was $16 \times 16 \text{ mm}^2$, which consisted of 16 SCD plates, each $4 \times 4 \text{ mm}^2$.

It is easily deduced what might be problematic with this method. It matches crystal characteristics at the interfaces between seeds. A lift-off process with ion implantation reduces complications while connecting multiple seeds. A high ion beam is injected onto the top surface of the substrate, and a graphitic layer is generated beneath the top surface. After this process, the SCD layer is grown onto the identical top surface. By selectively etching the graphite layer, we can obtain the SCD as a freestanding layer. What is more, the surface of the lifted-off plate was a part of the seed substrate. That means they have matching crystal characteristics on the surface. If this process is

repeated from a single seed, one can achieve many clones that share identical traits. Even this process still shows some imperfections along a line crossing the junction between seed crystals. If these areas differ significantly, they can be left out while producing power devices. In the worst case, almost 40% of the area has to be avoided. This varies depending on how many seeds were joined and what pattern was used [30, 21, 26, 1].

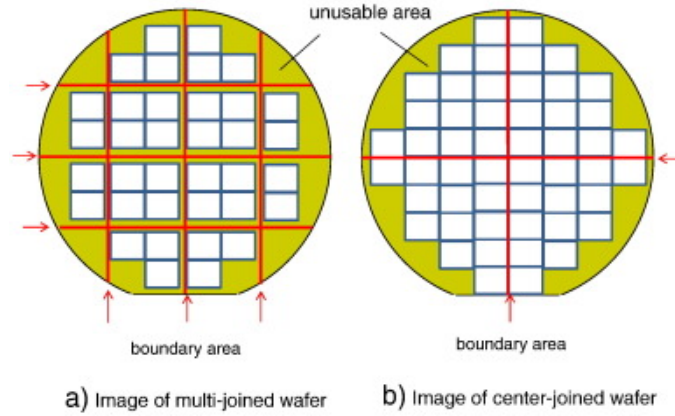


Figure 2.3: Diamond wafer using different mosaic techniques

Chapter 3

Atomic Force Microscopy

3.1 Basics and principles

Atomic force microscopy (AFM) is a type of scanning probe microscopy, which means it forms images of a surface by using a physical probe that scans the specimen. It is made out of six main components, which make the scanning possible. The first two are the cantilever and the tip at the end of the cantilever. Then there is a photo-detector and laser, isolating mechanisms, and last is Controller with a computer.

When it comes to scanning itself, it begins with the sample being mounted into the scanning chamber, where it has to be fixed. It is mainly done by a tripod and a slightly sticky surface so the sample will not move. Then we need to calibrate the laser. When the cantilever with tip moves across the surface, the laser is aimed towards the cantilever and is reflected to the photo-detector. It monitors and amplifies the cantilever deflection. The signal is then processed by the computer and shown on the computer screen. A feedback circuit connected to the deflection sensor adjusts the distance between the cantilever and the sample. It is essential to do so. If the tip touches the sample too hard, it could destroy its surface, or the tip might break.

AFM is capable of genuinely high resolutions in both vertical and lateral directions. The absolute limit of the vertical resolution is determined by the vertical scanner movement, which is $< 1\text{\AA}$ ($angström = 10^{-10}m$). AFM data are recorded digitally. The total number of available data points in the vertical direction can thus limit the resolution itself. The convention of a fixed number of bits over the full vertical range of the scanner determines it. Reducing the vertical range can increase the sampling resolution. It is typically around $0,3\text{\AA}$.

The radius of curvature of the end of the tip primarily determines lateral resolution. The sidewall angles of the tip will also determine its ability to probe high aspect ratio features. Typical tip radii quoted by the manufacturers for tapping mode tips are around $5 - 15\text{ nm}$, but these may increase quickly

with tip wear. The software may set the number of lines in an AFM scan and the number of samples per line.

As some basic knowledge, it might be interesting to note what forces we mostly come across and when. When the tip is moving closer and closer to the sample at the start of the scan, the Van der Waals forces with attractive tip-sample interaction are first to engage. This can be seen at the separation of 10 nm. When getting even closer, strong Coulombic repulsive forces will overcome the attractive ones and bend the cantilever away from the sample. In between, the tip might snap into actual contact with the sample; this occurs when $\frac{dF}{dz}$ exceeds the cantilever spring constant. (F is the force between the sample and the tip, and z is their vertical distance).

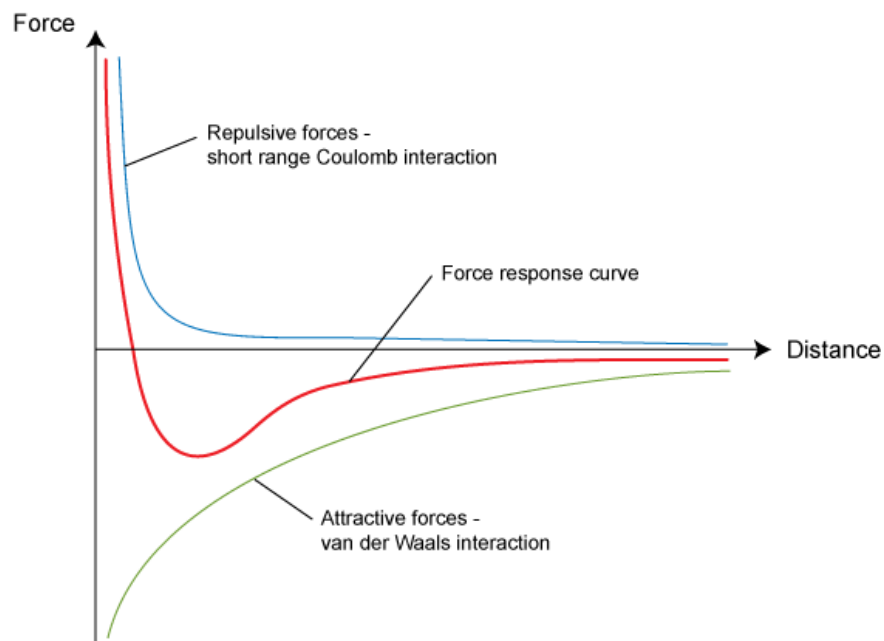


Figure 3.1: Force response curve of the tip [4]

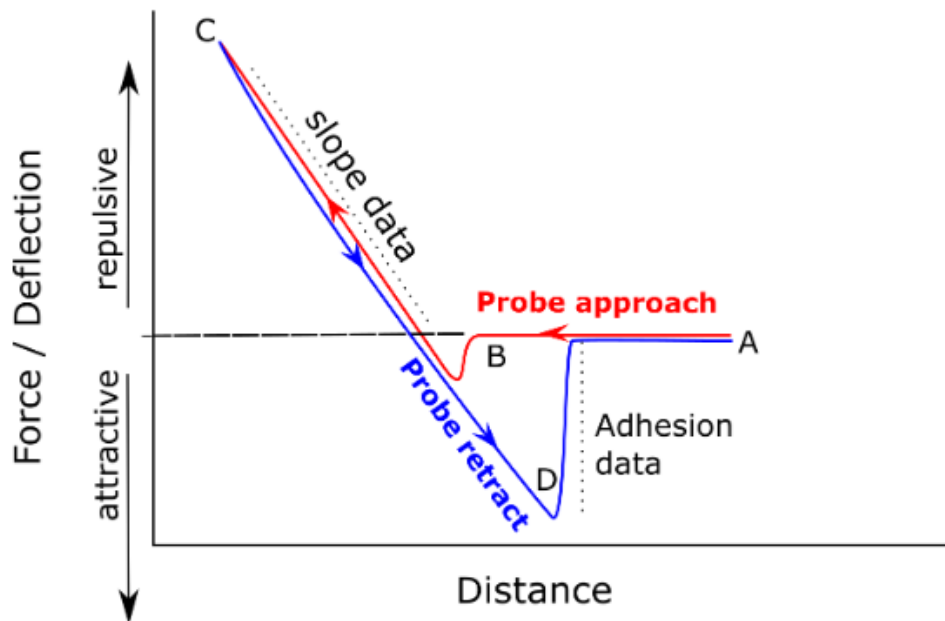


Figure 3.2: Force displacement curve [5]

In the picture above, we can see how the cantilever deflection will change while getting closer to the sample (red line) and then getting further from it (blue line).

- A) The tip is far from the sample, and the cantilever deflection is nearly zero.
- B) The cantilever deflects towards the sample due to the van der Waals forces. The tip then snaps into contact with the sample.
- C) After the contact, a positive deflection of the cantilever arises due to repulsive forces. This is the contact region of the force curve, where the elastic properties of the sample can be measured.
- D) Initially, the behaviour of the cantilever during withdrawal follows the trajectory described during the approach. Adhesion between tip and sample prevents separation. If a fluid exists on the sample, it will barely affect the attractive forces. However, the formation of a meniscus will contribute significantly to adhesion during withdrawal due to its high surface energy. Once the cantilever restoring force overcomes this adhesion force, the contact breaks.

It is obvious that overall behaviour is hysteretic.

While preparing the scan, we can choose from three scanning modes based on what results we need or what sample we are currently using.

First mode is **Contact mode**.

Here, the tip is scanned across the sample surface while monitoring the change in cantilever deflection. A feedback circuit is used to maintain a constant cantilever force (a constant deflection) to prevent major damage to the sample and the tip. This mode has its advantages and disadvantages, which are:

- + advantages: highest scan speed, easiest mode to set up for very rough samples
- disadvantages: usually lower resolution than other modes, high normal and lateral forces, possibility of damage to soft samples due to tip scratching the surface

Second one is **Tapping mode**.

The cantilever oscillates at or slightly below its resonance frequency with an amplitude ranging from 20nm to 100nm (usually, we use frequencies about 5 – 10% below resonant frequency). The tip lightly "taps" on the sample surface during scanning, contacting at the bottom of each swing. Changes in the tip-surface separation lead to changes in the resonant frequency of the cantilever given by:

$$\omega = \omega_0 \sqrt{1 - \frac{1}{k} \frac{\partial F}{\partial z}} \quad (3.1)$$

In addition, the oscillation amplitude is damped when the tip is closer to the surface. Thus, changes in the tip's oscillation amplitude can be used to measure the distance between the tip and the surface of the sample. In tapping mode, feedback is similarly critical. The detector senses a decrease in amplitude oscillation and sends a signal to the feedback circuit. The height of the cantilever is then adjusted by z-piezo so that oscillation recovers. As contact mode had its pros and cons, so does the tapping mode:

- + advantages: higher lateral resolution, reduced normal forces, lateral forces almost eliminated
- disadvantages: lower scan speed

The last primary mode is **Non-contact mode**. Non-contact mode employs an oscillating cantilever similar to tapping mode. The tip is oscillated with a small amplitude, usually slightly above its resonant frequency. The tip does not contact the surface. The cantilever's resonant frequency is decreased by the van der Waals forces (the decrease in resonant frequency causes the amplitude of oscillation to decrease, too) and by other long-range forces which extend above the surface. In many cases, the fluid contaminant layer is substantially thicker than the range of the van der Waals force gradient. Therefore, attempts to imagine the actual surface with NC-AFM fail as the oscillating probe becomes trapped in the fluid layer or hovers beyond the effective range.

- + advantages: minimal lateral and normal forces, atomic resolution in UHV (ultra-high vacuum)
- disadvantages: limited resolution in air due to fluid contaminant layer on most surfaces, lowest scan speeds

[31, 32, 33, 34]

3.2 Other capabilities of AFM

Now that we know the basic principles of how AFM works, we could also mention why it is so widely used and what else we can do except generate surface topography. AFM can be used to look at insulating samples, too, such as polymers, ceramics or bio-materials, without any special preparation. It is even possible to imagine it in a liquid environment. Numerous techniques have been developed to allow material properties to be imagined simultaneously with topography. In these techniques, the lift mode is used. Its principle is pretty straightforward, AFM first records topographical data in tapping mode on one trace and retrace. The tip then rises to keep the constant height over the surface and scans the same area with a different approach.

MFM: magnetic force microscopy

When using MFM, the tip is coated with a thin ferromagnetic film. The magnetic field between the tip and the film depends on the tip-sample separation and the sample's magnetic properties. During the lift scan, the tip-sample distance is constant and as the tip passes over different magnetic domains, the force gradient changes – changing the natural oscillation frequency. There are three possible methods to detect the changes in the natural frequency of the tip [35]:

- Amplitude detection: the shift in amplitude at a fixed drive frequency
- Phase detection: the shift in phase at the fixed drive frequency
- Frequency modulation: a feedback loop modulates the drive frequency to keep the cantilever's phase lag at 90° relative to the drive, corresponding to the resonance

EFM: electric force microscopy

As with MFM, we detect changes in the force gradient due to local changes in materials properties, except here, the forces involved are electrostatic rather than magnetic. Tips coated with a conductive film are used, and a DC bias may be applied. Attractive forces reduce the cantilever resonant frequency. As with MFM, changes in resonant frequency may be assessed using phase detection, amplitude detection, or frequency modulation [36].

Kelvin probe force microscopy

Also known as Surface Potential Microscopy. Lift mode is used. On the first pass, the topography is measured, on the second pass, a constant height above the sample is maintained, and the cantilever is not vibrated. Instead, an oscillation voltage is applied:

$$V = V_{AC} \sin(\omega t) \quad (3.2)$$

this creates an oscillating electric force at the frequency ω on the cantilever. The oscillating force has the following amplitude:

$$F = \frac{\partial C}{\partial z} \Delta V_{dc} V_{ac} \quad (3.3)$$

where $\frac{\partial C}{\partial z}$ is the vertical derivative of the tip-sample capacitance and

$$\Delta V_{dc} = V_{tip} - V_{sample} \quad (3.4)$$

When the tip and sample are at the same DC voltage, the cantilever experiences no oscillating force. By adjusting the DC voltage on the tip until the oscillation amplitude equals zero, the effective local surface potential on the sample may be determined. The surface potential image is a map of V_{sample} over the surface [37, 34].

Lithography

AFM can not only be used to determine specific characterisations of materials but also to change the sample surface in either destructing or building way. AFM typically operates in contact mode when used in this way, scratching the surface to carve specific patterns onto it. For this use, special tough tips are used. For local oxidation nanolithography, it is necessary to have relative humidity in the chamber with a sample between 30 to 60%. A voltage pulse is applied between a conductive AFM tip and the sample. This voltage induces the formation of a water bridge between the tip and sample whenever the amplitude exceeds a certain threshold voltage. Then the applied voltage causes an oxidation reaction by breaking the covalent bonds in the water molecules. Only a tiny voltage is needed (between 5 to 50V) since the distance between the tip and sample is small. Thus created electric field is enormous [38, 39].

Even more, techniques can be used with AFM to acquire other needed information about samples such as capacitance, resistance, conductivity, currents in piko Ampers and others. AFM can also measure the mechanical properties of samples, such as friction forces. It can be used in many ways, and its impact on technology and science is tremendous.

Chapter 4

Raman Spectroscopy

4.1 Basics and principles

When light scatters, the wavelength of the light, thus its energy, can be altered by the scattering process. With a very small chance, scattered photon loses part of their energy to the molecule and changes its wavelength. Indian scientist C. V. Raman for the first time observed this effect, and he even won a Nobel prize in 1930 for this discovery. If a photon is scattered without losing energy, we call the process Rayleigh scattering or elastic scattering. If it does, we call it Raman scattering or inelastic. If Raman scattering happens, the scattered photon carries a different amount of energy. This difference is called Raman shift and is transferred into molecular vibrations. Vibration energy can only take certain separate states. The ground state is zero with some vibration energy, and every other higher state with stronger vibration. If a photon hits a molecule and passes some energy to it, it goes higher in vibration states. The photon will, in return, scatter with less energy, thus creating a longer wavelength. That is how Raman scattering happens. The energy difference between state zero and state one depends only on the natural frequency of the vibration. This is very specific, and we can determine what molecules we have just based on its Raman shift.

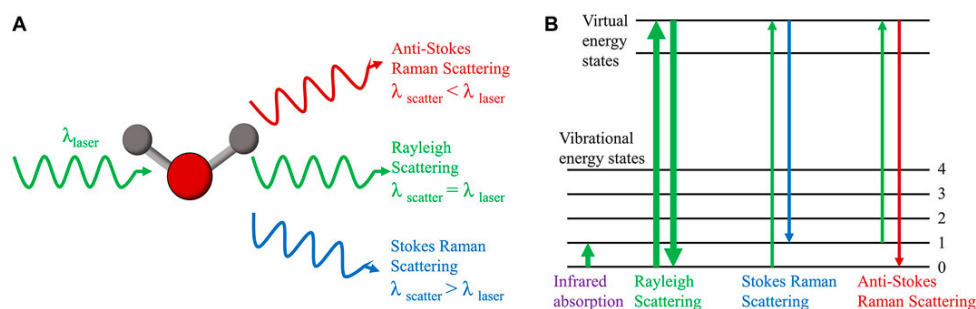


Figure 4.1: Principle of Raman scattering [6]

To see the Raman effect, we need four main components. A laser, an optical filter, a spectrograph and a CCD detector. It is essential to all photons with the same amount of energy, in other words the same wavelength. The optical filter only passes through the Raman scattered light and reflects Rayleigh scattered light. After passing through the filter, we need to know the exact wavelengths of photons. That is what a spectrograph is there for. It guides the photons in different directions according to their wavelengths. These then fall on distinct positions on the CCD detector; thus, we capture a photo of Raman's scattered light. The more photons reach the CCD, the higher the light intensity and, eventually, the brighter spot. As a result, we have the Raman scattering intensity as the function of wavelength. However, we make it more complex and make it into the function of the inverse centimetre, which is also called wavenumber. This creates a very simple Raman spectrum. It has one significant advantage. Unlike the wavelength, the wavenumber is directly proportional to the photon's energy. By defining the laser wavelength as zero in the Raman spectrum, we make the relative number of Raman scattering proportional to the energy between the vibrational states. This way, the laser wavelength no longer plays a role in results. This also means that we can use any laser wavelengths, which will always lead to the same Raman shift for the same vibrational frequency.

During the Raman experiment, a molecule can absorb the high-energy photon and achieve an electronically excited state. From this state, it may relax back to the ground state and emit a photon with less energy and a longer wavelength. It is called the fluorescence effect. It is fundamentally different from the Raman effect, but both result similarly. This means that even these photons can get through the filter. The fluorescence spectrum appears much broader than Raman and holds no information about molecular vibration. If unexpected fluorescence happens, mild interferences can be removed by data processing. However, light emitted during fluorescence is much more intense than Raman scattered light. This might lead to flooding the detector and making results unreadable. We can avoid this effect in many ways. The easiest of them is just by changing the wavelength of the light from the laser. This is primarily done to lower energy lights because they usually do not excite molecules electronically. Another way is used when the sample itself is coloured, and then we use the light of the same colour since it is less likely to get absorbed and cause the fluorescence effect.

This is not the only factor influencing our laser selection. We know that the shorter the wavelength, the stronger the scattering effect. This is reflected in the sensitivity of the scan itself in a way that a laser with a shorter wavelength can provide us with more Raman signal. But these photons have more energy and are more likely to get involved in the fluorescence effect. Violet light is thus very rarely used in Raman spectroscopy. Another limiting factor is detector sensitivity. The usual CCD detector can detect Raman peak below 1100nm. Anything beyond that will need an IR detector. These typically

possess less sensitivity and will lead to longer and lower-quality scans. Most Raman spectrometers use lasers ranging from 450nm to 800nm to prevent most of the negative effects. The 532nm green laser and 785nm NIR laser light are two widely used. A less impactful factor is heating, but it must be addressed. [40, 41, 42, 43]

4.2 Other capabilities of Raman spectroscopy

As AFM did have more ways of use, so does the Raman spectroscopy. These have been developed throughout the years to specify the measures or to improve some specific capabilities. Mainly enhancing sensitivity, spatial resolution, or even acquiring specific information atop of what Raman is originally meant to, like resonance frequency of the sample.

Resonance Raman spectroscopy

As we know, Raman scattering is usually very weak. Therefore a Resonance Raman spectroscopy (RRS) can be used. It is necessary to know some basic information about the sample ahead of measuring it. It requires the laser excitation frequency to be chosen very close to the frequency of an electronic transition of the molecules. RRS can enhance the Raman scattering intensity by a factor of $10^2 - 10^6$ and thus improve the signal-to-noise ratio. This can also be used to shorten exposure times, leading to much faster spectral acquisition times. The most significant enhancement occurs when the laser frequency matches the samples. If there are larger molecules, we can even confirm the change in electron density to particular parts. This also can help with identifying unknown substances in samples. RRS is very popular and widely used in biological materials. For example, a chromophore is part of a molecule that is responsible for its colour. This means that if we can select the correct frequency, we can better analyse coloured samples and make interpretation much more effortless. One drawback of RRS is increased fluorescence which can swamp the Raman signal. When matching the laser to an absorption band, absorption will occur, meaning there is a high chance of fluorescence obscuring the Raman peaks. The interference of fluorescence limits the number of molecules studied by Resonance Raman spectroscopy. [42, 44]

Surface - Enhanced Raman spectroscopy

In Surface - Enhanced Raman spectroscopy (SERS), we place the measured molecule near a metal surface. This can dramatically increase the Raman signal. The enhance factor can be up to 10^{11} , which means we can detect even single molecules. There are several factors supporting this enhancement.

- The distance to the metal surface:

The molecule of interest must be close to the surface for signal enhancement to occur

- Details about the metal surface:
Morphology and roughness of surface determine how close and how many molecules can be near a particular surface area
- The properties of the metal:
Greatest enhancement occurs when the excitation wavelength is near the plasma frequency of the metal
- The relative orientation of the molecule to the normal of the surface:
The polarizability of the bonds within the molecule can be affected by the electrons in the surface of the metal

The exact mechanism of SERS enhancement remains an active research topic even today. Two significant factors contribute to enhancement, which is chemical and electromagnetic enhancement. The chemical mechanism is now thought to contribute an average enhancement factor of 100. A charge-transfer state is created between the metal and adsorbate molecules. In a manner analogous to that observed in resonance Raman spectroscopy, the existence of this charge-transfer state increases the probability of a Raman transition by providing a pathway for resonant excitation. This mechanism is site-specific and analyte-dependent. The molecule must be directly adsorbed to the roughened surface to experience the chemical enhancement.

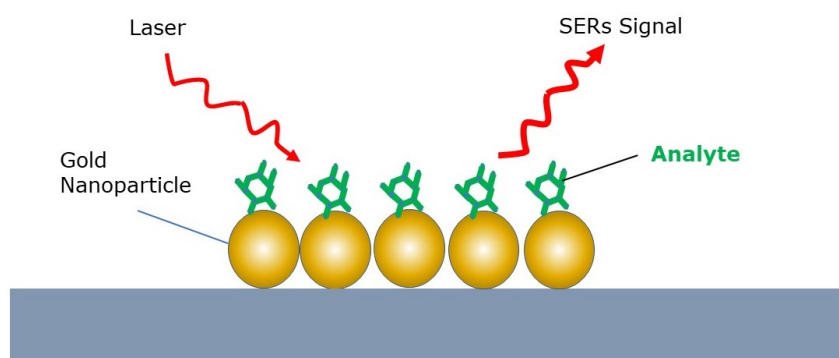


Figure 4.2: Illustration of SERS principle [7]

In electromagnetic enhancement, one must consider the nanoscale features' size, shape and material. These characteristics determine the resonant frequency of the conduction electrons in a metallic nanostructure. When electromagnetic radiation with the same frequency is incident upon the structure, the electric field of the radiation drives the conduction electrons into collective oscillation. Two consequences emerge: selective absorption and scattering of the resonant electromagnetic radiation and generation of large electromagnetic fields at the surface of the roughness feature. Whole electromagnetic enhancement relies on Raman-active molecules being confined within these fields. This factor contributes to enhancement in orders of 10,000s.

The SERS technique has many advantages but also many limitations. Because the SERS analyte must be on or near a noble metal, which provides non-radiative pathways for the decay of excited states, fluorescence interference is strongly quenched. With the appropriate instrumentation, low-frequency vibrational modes beyond the range of IR absorption spectroscopy can be observed with SERS. Furthermore, the abrupt decay of the electromagnetic fields ensures that only adsorbate molecules on or near the noble-metal substrate (within 4 nm) are probed. The inherent limitations of the technique must also be considered. The most apparent constraint lies in the limited substrate choices that exhibit LSPR behaviour. The most commonly used substrates are made of silver, gold, and copper. Experimental and theoretical work has also demonstrated the SERS phenomenon on aluminium, caesium, gallium, indium, lithium, platinum, potassium, rhodium, rubidium, and sodium substrates. However, other materials are only usable if applied as thin coatings on SERS-active materials. [45, 46, 47]

Correlative Raman imaging

Measuring with Raman spectroscopy can be combined with other microscopy techniques to join their results into a complex sample characterisation. Common examples of correlative microscopy are atomic force microscopy (Raman-AFM) or scanning electron microscopy (Raman-SEM).

Chapter 5

Experimental Part

5.1 Theoretical introduction

In fabricating high-performance diamond semiconductor devices, careful control over dopant incorporation, unwanted defects in epitaxial layers, and electrical properties are crucial. Conventionally studied (100) and (111) epitaxial layers each show their pros and cons. For (100) homo-epitaxial layers, it is easy to dope them with boron, but they suffer at low phosphorus incorporation, thus poor n-type electrical properties. (111) homo-epitaxial layers can be, on the contrary, grown with higher phosphorous concentrations, having superior n-type properties, but are more susceptible to the formation of twins and growth defects on the surface. Also, poorer p-type electrical properties can be observed. Recently, the deposition of epitaxial diamond layers has been studied on some vicinal surfaces such as (113), (110) or (115). One such research is also being done here at Czech Technical University in Prague at the Department of Microelectronics [48]. A closer look at the surface characterisation and the boron incorporation homogeneity was determined. Furthermore, based on the results, a closer look at the vicinal (113) surface has been made. Here, different properties have been studied by AFM, electron microscopy, secondary ion mass spectroscopy and Raman spectroscopy. Results show high deposition rates, atomically flat surfaces, excellent electrical properties and high boron incorporation efficiency [49]. One year later, the article was published on low-resistance ohmic contacts on the same homoepitaxial diamond layer orientation [50].

In this experimental part, we will look closely at four diamond samples, each with a different orientation. All of them were made by CVD at Institute of Physics of the Czech Academy of Sciences on HPHT diamonds. Each sample was first observed under an optical microscope and then carefully selected the area for further scanning. Surface characterisation was done by Atomic Force Microscopy (AFM) here at CTU in NanoLab, placed at the department of microelectronics. Model specifications are NT-MDT Ntegra Prima. On each sample, Raman spectroscopy was done, observing Raman shift and potential impurities or occurrence of fluorescence effect on surfaces. Raman scans were done by Raman Spectrometer from Renishaw inVia Qontor

with three possible excitation lasers – 532nm, 633nm and 830nm, which is located in NanoLab in CTU too.



Figure 5.1: AFM microscope from NTEGRA [8]



Figure 5.2: Raman spectroscopy microscope from Renishaw [9]

As mentioned above, the laser wavelength is not influencing results in the Raman shift. Thus all scans have been done only by 532nm laser, which was chosen because of the least effect on the fluorescence occurrence on diamonds. For each sample, a picture from an optical microscope focused on the scanning area will be shown, and then AFM profiles and Raman spectra will be shown. Samples with orientation (111), (100) and (113) will be compared with the results from [NANOCON paper]. For the last sample with orientation (115),

only observation will be described, and some conclusions about fabrication semiconductors will be made.

5.2 Sample properties

5.2.1 (100) oriented homo-epitaxial boron-doped diamond

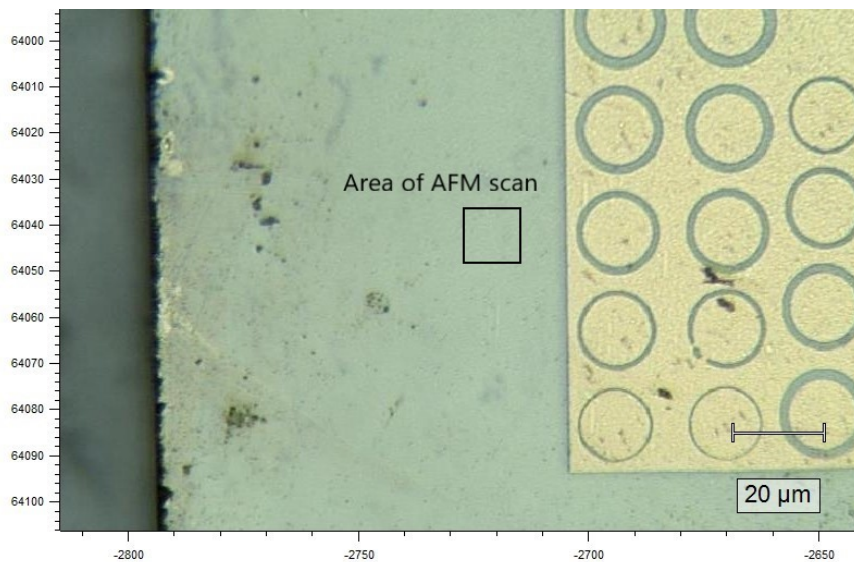


Figure 5.3: Close look at the (100) sample under build-in optical microscope in Raman spectroscopy with highlighted area of scan ($8 \times 8 \mu m$)

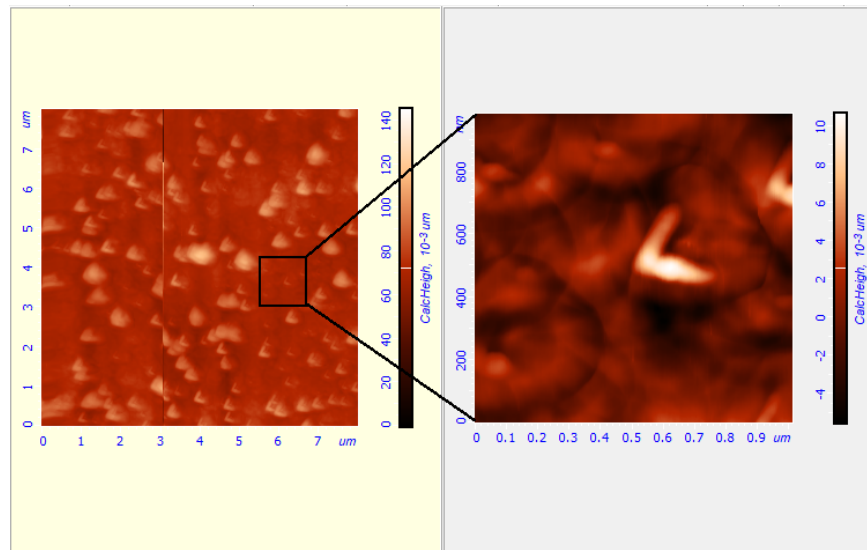


Figure 5.4: AFM scan of highlighted area with next, more detailed scan of what appeared to be narrow surface

Although on the first sight from optical microscope the surface appears to be clear and narrow, after closer examination with AFM, we can clearly see the opposite. Throughout whole there are frequently and irregularly scattered 'L-shaped' structures. They appear to be approximately half μm in width and under 150 nm in height. After more detailed scan on what again appeared to be decently clear surface, we can see this structures too in quite lesser scaling. Now reaching 0.2 μm in width and under 10 nm in height.

In the picture of the 8x8 μm scan we can observe this wall going from top to the middle of the sample at about 3 μm from the left side. This was most probably caused by some kind of micro dirt or dust that attached to the tip of the AFM and got dragged along the surface. Fortunately it was not stuck for too long and thus can the scan still be used as an example of the surface.

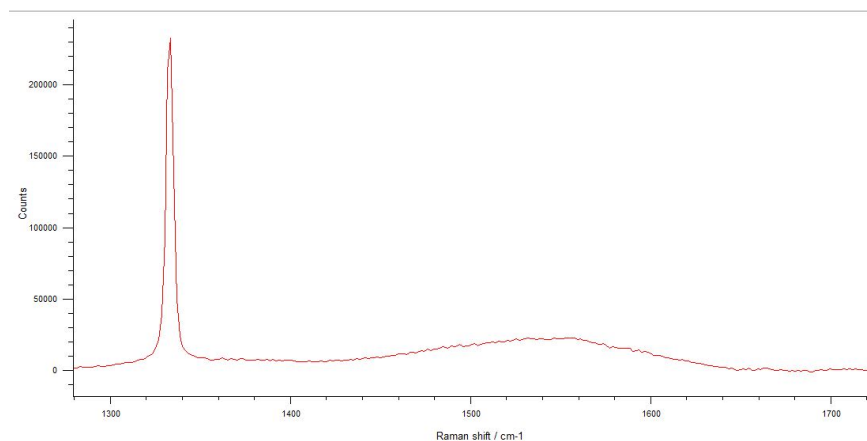


Figure 5.5: Raman scan of the sample at random selected point

Raman spectra shows characteristic peak at 1 332 cm^{-1} and what appears

to be very slight fluorescence effect. Comparing these observations with ones obtained by CTU research [48], we can see differences. Observed structures are quite similar in shape, but not in size. while here we can see at maximum orders of μm , those observed by CTU were around $100 \mu m$ in base.

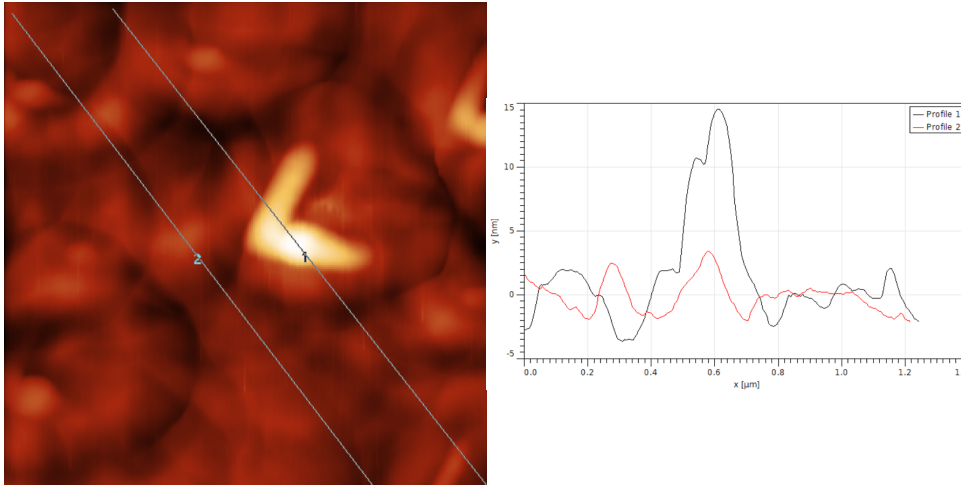


Figure 5.6: Height profile comparison of one going pass by the L-shaped structure and one going through it

5.2.2 (111) oriented homo-epitaxial boron-doped diamond

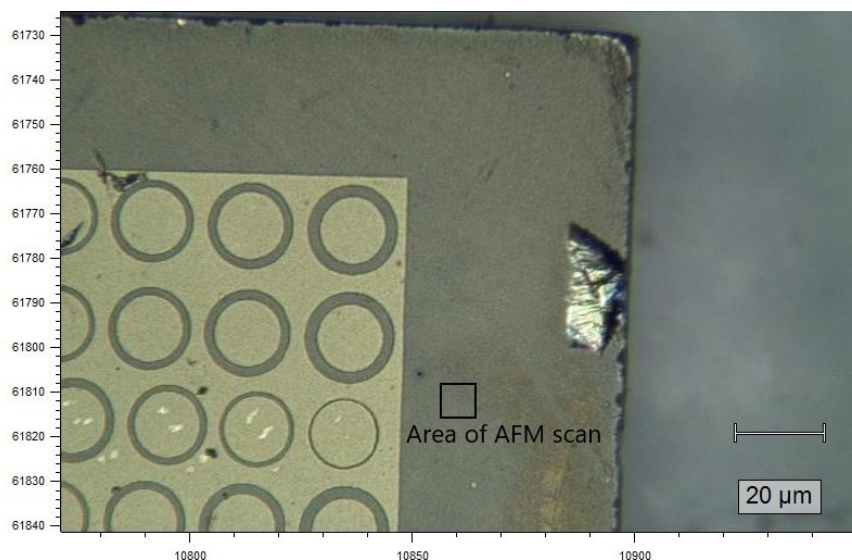


Figure 5.7: Close look at the (111) sample under build-in optical microscope in Raman spectroscopy with highlighted area of scan

The (111) oriented homo-epitaxial diamond layer optically appears to be very uniform over its surface. Even under closer AFM scan, there are only minor hills spread over whole surface quite irregularly, but frequently. Since (111) orientation is inclined, further correction with flattening of surface was done. After this process we can see what appeared to be over $2\mu\text{m}$ in height was just the slope and thus hills only reach up to 60 nm in height. While doing the height profile and trying to avoid major structural defects a line with under 10 nm in height can be achieved. Thus surface in this orientation can be truly flat. Another polishing process could solve these little inequalities. Raman scan again shows typical peak at 1332 cm^{-1} , but also a little more significant fluorescence than in (100) oriented surface. These observations can be compared to those acquired by CTU research only their surface had less defects [48].

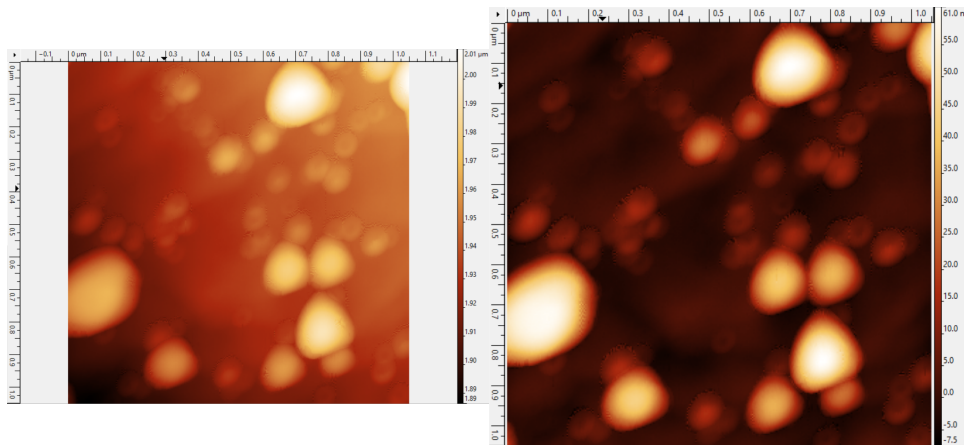


Figure 5.8: Comparison of differences between uncorrected (left) and corrected (right) slope of the scan on AFM sample

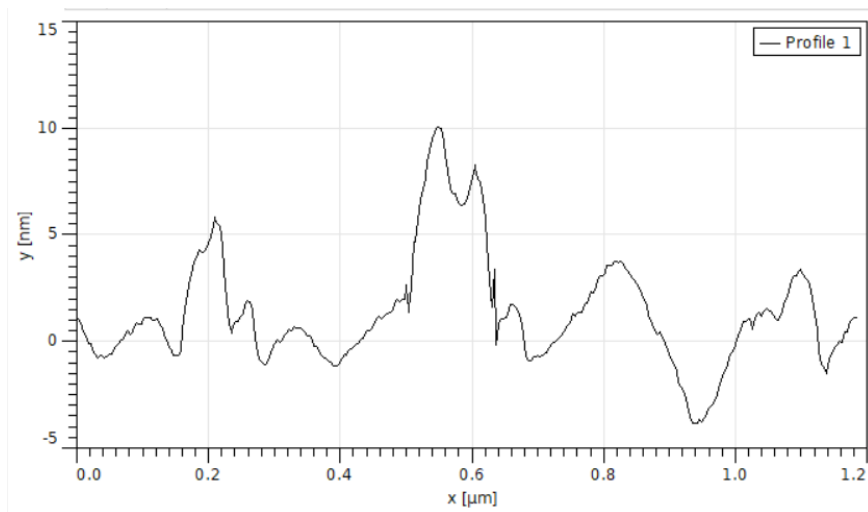


Figure 5.9: Height profile of selected line at (111) orientation

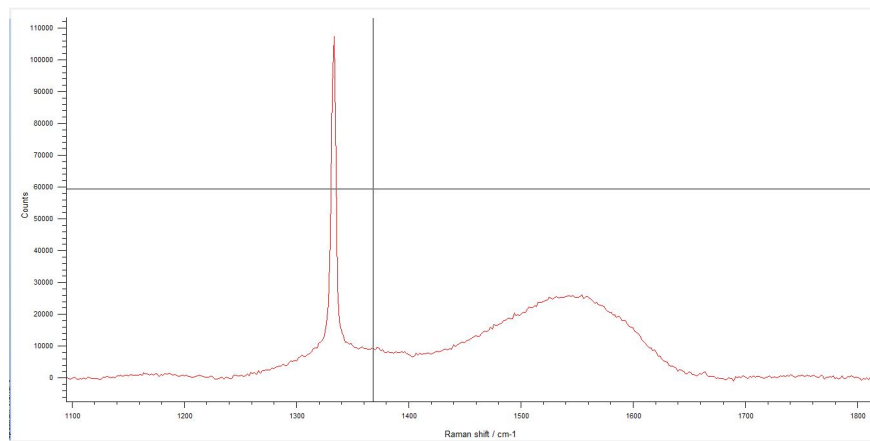


Figure 5.10: Raman spectra of randomly selected point in the scanning area of the (111) sample

5.2.3 (113) oriented homo-epitaxial boron-doped diamond

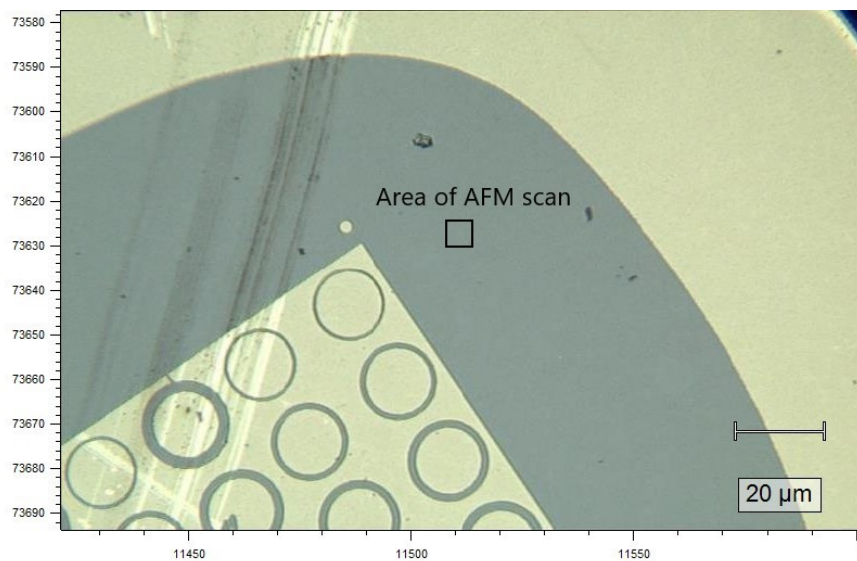


Figure 5.11: Close look at the (113) sample under build-in optical microscope in Raman spectroscopy with highlighted area of scan

On the (113) oriented homo-epitaxial diamond we can observe very rarely occurring structural anomalies. These are small in width, not over $0.2 \mu m$, but quite high in comparison. From height profile we can see they can reach over $45 nm$. Referring to the CTU research, (113)-oriented boron-doped diamond surface should be flat and homogeneous with near to none linear defects. If we neglect these three appearing defects, the surface is not more than $4 nm$ in

height which could correspond to what it should look like. 3D image shows these differences even better. On contrary to (100) and (111) orientation, Raman scan shows no signs of fluorescence and again the same peak at $1\,332\text{ cm}^{-1}$.

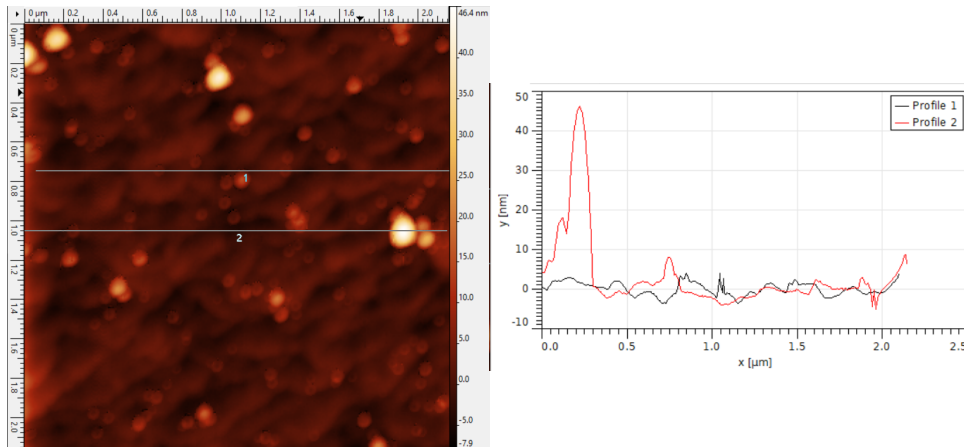


Figure 5.12: Height profile with shown lines on AFM scan of the sample

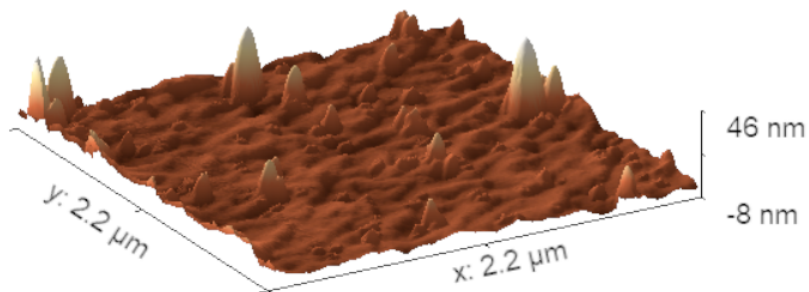


Figure 5.13: 3D profile of scanned area ($2.2 \times 2.2\ \mu\text{m}$)

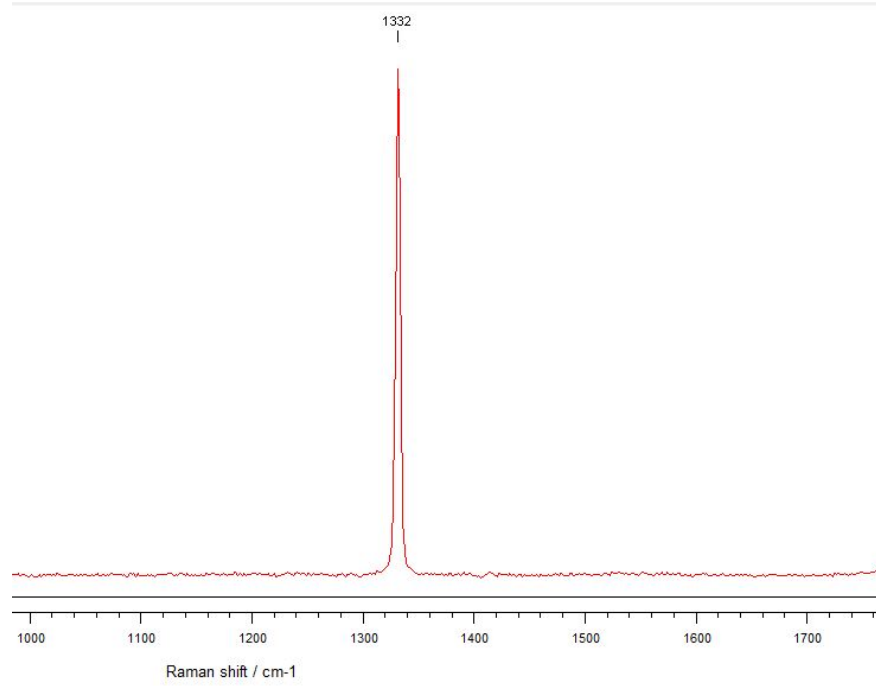


Figure 5.14: Raman spectra of (113)-oriented homo-epitaxial boron-doped diamond with no sign of fluorescence

5.2.4 (115) oriented homo-epitaxial boron-doped diamond

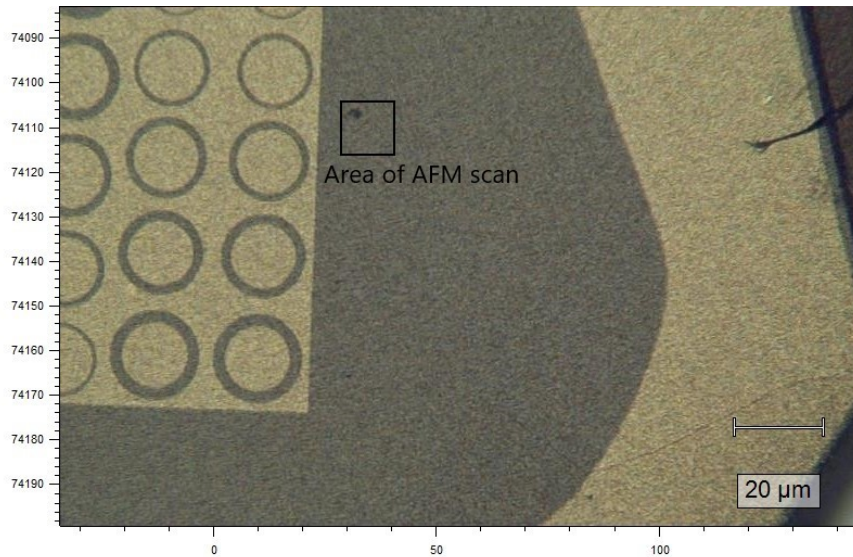


Figure 5.15: Close look at the (115) sample under build-in optical microscope in Raman spectroscopy with highlighted area of scan

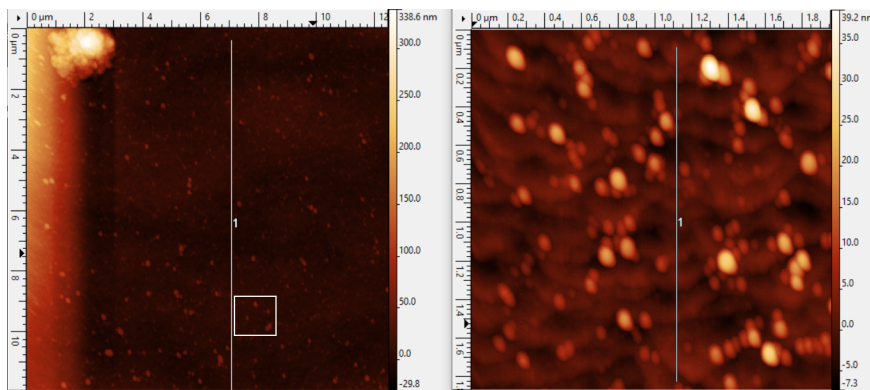


Figure 5.16: AFM scan of larger area 12x12 μm and then detailed scan of partly-selected area of 2x2 μm

Scan on (115) oriented homo-epitaxial boron-doped diamond was done next to optically visible defect on surface. We can deduce from scan that it is definitely not a scratch, but possibly some left-overs after deposition or coating, although it is still only 338 nm in height. Rest of the surface is quite roughly sprinkled with small seeds of defects. In the closer look we can see they are not more than 40 nm in height, but still very frequent and even the rest of the surface is filled with more, smaller seeds of irregular shape. From profile we can deduce that even though there are many defects, none of them

are significantly different and there are no spikes occurring on the sample surface. From all the samples, this one show disturbingly huge amount of fluorescence at $1\ 544\ \text{cm}^{-1}$ Raman shift.

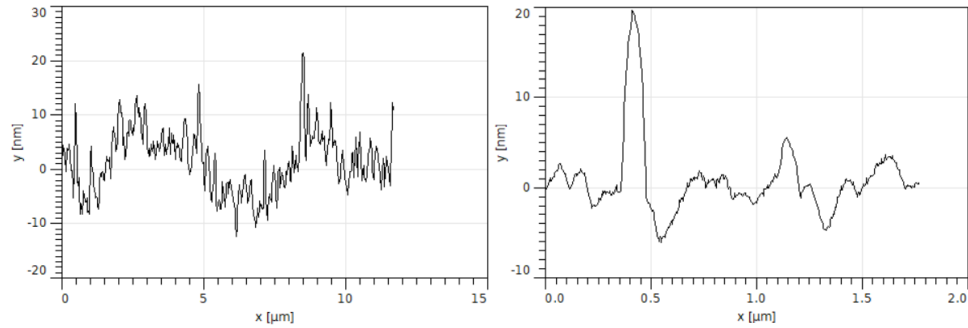


Figure 5.17: Comparison of height profiles with shown lines on AFM scans

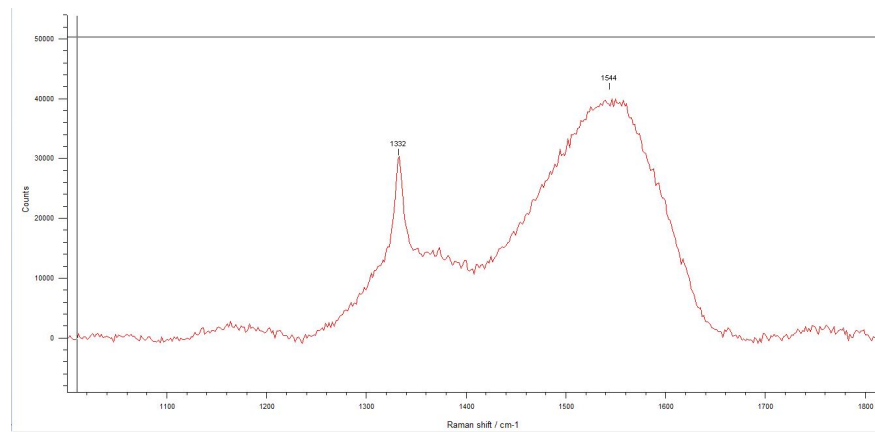


Figure 5.18: Raman spectra of (115) oriented homo-epitaxial boron-doped diamond

Chapter 6

Conclusion

Electronic semiconductor devices are becoming smaller and faster each year. With more extreme conditions during use, more demands rise for reliable and sustainable materials alongside with the need for more efficient fabrication. Synthetic diamonds show promising future in both aspects, especially for the applications in power electronics. Thanks to advanced growing and clearing methods we can access samples with different oriented homo-epitaxial boron-doped diamonds. Even though diamonds are being studied for many years, further development is nowhere near ending and there is still a lot to be either more specified or even discovered.

In this thesis, the basic properties and characterisation of synthetic diamonds were described, and many advantages were highlighted, compared to different challenges that can occur during processes. An overview of applications was given, focusing on the industry of semiconductor devices. Using atomic force microscopy and Raman spectroscopy, four samples were analysed. Each of the studied surface orientations (100), (111), (113) and (115) show narrow band structure with defect occurrences. These defects are most likely caused by inhomogeneous boron incorporations or point defects such as vacancies or interstitials in dependence on the epitaxial growth direction. This is further supported by Raman spectrometer scans which show different, but observable fluorescence effects occurring in samples. The highest fluorescence is on sample with (115) growth orientation and its intensity at $1\ 544\ \text{cm}^{-1}$ Raman shift actually exceeds Raman peak for diamond at $1\ 332\ \text{cm}^{-1}$. This sample also had the highest density of surface defects, but they were not the highest ones. At the sample with growth orientation (111) with second most density of defects along with the highest ones reaching up to 60 nm. Peak of fluorescence was also around $1\ 550\ \text{cm}^{-1}$ Raman shift. Very weak fluorescence occurred at sample (100), once again at around $1\ 550\ \text{cm}^{-1}$ Raman shift. Here, surface was rough, but defects differed in height quite a lot from smallest around 10 nm to the highest around 130 nm. It looks like the more dense defects there are, the more intense the fluorescence effect is. For the sample with growth orientation of (113), none fluorescence was observed, but defects were the least dense here.

However, it appears that positive properties of diamond structures over-

6. Conclusion

whelm those limiting ones, moreover, they can be reduced to even lesser impact on industrial application. This means that diamonds have promising future in semiconductor industry, but more research is needed to further investigate all properties and develop more applicable solutions.



Bibliography

- [1] GIA. Is there a difference between natural and laboratory-grown diamonds?, 2023. Diamond Morphology.
- [2] Graham Tom Consultancy. Synthetic diamonds, 2022. Production of Synthetic Diamonds.
- [3] Hitoshi Umezawa, Masanori Nagase, Yukako Kato, and Shin ichi Shikata. High temperature application of diamond power device. *Diamond and Related Materials*, 24:201–205, 2012.
- [4] University of Cambridge. Tip surface interaction of afm, 2004-2023. Tip Surface Interaction of AFM.
- [5] AFM Workshop. Afm workshop, 2010-2023. Measuring Force-Distant Curves with AFM.
- [6] Kunxiang Liu, Qi Zhao, Bei Li, and Xia Zhao. Raman spectroscopy: A novel technology for gastric cancer diagnosis. *Frontiers in Bioengineering and Biotechnology*, 10, 2022.
- [7] AZO nano. Surface enhanced raman spectroscopy, 2000-2023. Surface Enhanced Raman Spectroscopy.
- [8] Ntegra Prima. Afm workshop, 2021. online from: https://www.ntmdt-si.com/data/media/images/products/ntegra/prima/integra_new.jpg.
- [9] Renishaw. Renishaw apply innovation, 2021. online from: <https://www.renishaw.com/media>.
- [10] Tesfaye Ayalew. *SiC semiconductor devices technology, modeling and simulation*. PhD thesis, 2004.
- [11] RockHer. How diamonds are mined, 2022. How Diamonds are Mined.
- [12] H Tracy Hall. Ultra-high-pressure, high-temperature apparatus: the“belt”. *Review of Scientific Instruments*, 31(2):125–131, 1960.
- [13] FP Bundy, H Tracy Hall, HM Strong, et al. Man-made diamonds. *nature*, 176(4471):51–55, 1955.

- [14] Tairus. High pressure high temperature (hpht) method, 2021. High Pressure High Temperature (HPHT) method.
- [15] Robert J Nemanich, John A Carlisle, Atsushi Hirata, and Ken Haenen. Cvd diamond—research, applications, and challenges. *Mrs Bulletin*, 39(6):490–494, 2014.
- [16] Shinichi Shikata. Single crystal diamond wafers for high power electronics. *Diamond and Related Materials*, 65:168–175, 2016. Special Issue “26th International Conference on Diamond and Carbon Materials – DCM 2015”.
- [17] Konstantin Iakoubovskii and GJ Adriaenssens. Optical characterization of natural argyle diamonds. *Diamond and Related Materials*, 11(1):125–131, 2002.
- [18] Jan Isberg, Johan Hammersberg, Erik Johansson, Tobias Wikstrom, Daniel J Twitchen, Andrew J Whitehead, Steven E Coe, and Geoffrey A Scarsbrook. High carrier mobility in single-crystal plasma-deposited diamond. *Science*, 297(5587):1670–1672, 2002.
- [19] K. Somogyi. Classical approximations for ionised impurity scattering applied to diamond monocrystals. *Diamond and Related Materials*, 11(3):686–691, 2002. 12th European Conference on Diamond, Diamond-Like Materials, Carbon Nanotubes, Nitrides Silicon Carbide.
- [20] BA Fox, ML Hartsell, DM Malta, HA Wynands, C-T Kao, LS Plano, GJ Tessmer, RB Henard, JS Holmes, AJ Tessmer, et al. Diamond devices and electrical properties. *Diamond and related materials*, 4(5-6):622–627, 1995.
- [21] Chris J.H. Wort and Richard S. Balmer. Diamond as an electronic material. *Materials Today*, 11(1):22–28, 2008.
- [22] Shinichi Shikata. Single crystal diamond wafers for high power electronics. *Diamond and Related Materials*, 65:168–175, 2016. Special Issue “26th International Conference on Diamond and Carbon Materials – DCM 2015”.
- [23] A Vescan, I Daumiller, P Gluche, W Ebert, and E Kohn. Very high temperature operation of diamond schottky diode. *IEEE Electron Device Letters*, 18(11):556–558, 1997.
- [24] F Roccaforte, G Brezeanu, PM Gammon, F Giannazzo, S Rascunà, and M Saggio. Schottky contacts to silicon carbide: Physics, technology and applications. *Advancing Silicon Carbide Electronics Technology, I: Metal Contacts to Silicon Carbide: Physics, Technology, Applications*, pages 9781945291852–3, 2018.

- [25] Stephen AO Russell, Salah Sharabi, Alex Tallaire, and David AJ Moran. Hydrogen-terminated diamond field-effect transistors with cutoff frequency of 53 ghz. *IEEE Electron Device Letters*, 33(10):1471–1473, 2012.
- [26] Hitoshi Umezawa. Recent advances in diamond power semiconductor devices. *Materials Science in Semiconductor Processing*, 78:147–156, 2018. Wide band gap semiconductors technology for next generation of energy efficient power electronics.
- [27] William Joseph Yost. Assembling the building blocks for diamond electronics. *MRS Online Proceedings Library (OPL)*, 956, 2006.
- [28] Hideaki Yamada, Akiyoshi Chayahara, Yoshiaki Mokuno, Nobuteru Tsubouchi, Shin ichi Shikata, and Naoji Fujimori. Developments of elemental technologies to produce inch-size single-crystal diamond wafers. *Diamond and Related Materials*, 20(4):616–619, 2011.
- [29] Y. Mokuno, A. Chayahara, H. Yamada, and N. Tsubouchi. Improving purity and size of single-crystal diamond plates produced by high-rate cvd growth and lift-off process using ion implantation. *Diamond and Related Materials*, 18(10):1258–1261, 2009.
- [30] Hideaki Yamada, Akiyoshi Chayahara, Yoshiaki Mokuno, Hitoshi Umezawa, Shin-ichi Shikata, and Naoji Fujimori. Fabrication of 1 inch mosaic crystal diamond wafers. *Applied Physics Express*, 3(5):051301, 2010.
- [31] NanoSurf AG. How does afm work, 2022. AFM principles.
- [32] Park Systems. How afm works, 2023. Raman Spectroscopy.
- [33] ERNST Meyer. Atomic force microscopy. *Progress in surface science*, 41(1):3–49, 1992.
- [34] Daniel Rugar and Paul Hansma. Atomic force microscopy. *Physics today*, 43(10):23–30, 1990.
- [35] U Hartmann. Magnetic force microscopy. *Annual review of materials science*, 29(1):53–87, 1999.
- [36] Paul Girard. Electrostatic force microscopy: principles and some applications to semiconductors. *Nanotechnology*, 12(4):485, 2001.
- [37] Marco Salerno and Silvia Dante. Scanning kelvin probe microscopy: challenges and perspectives towards increased application on biomaterials and biological samples. *Materials*, 11(6):951, 2018.
- [38] A Notargiacomo, V Foglietti, E Cianci, G Capellini, M Adami, P Faraci, F Evangelisti, and C Nicolini. Atomic force microscopy lithography as a nanodevice development technique. *Nanotechnology*, 10(4):458, 1999.

I. OSOBNÍ A STUDIJNÍ ÚDAJE

Příjmení: **Stanko** Jméno: **Rudolf** Osobní číslo: **492227**
Fakulta/ústav: **Fakulta elektrotechnická**
Zadávající katedra/ústav: **Katedra radioelektroniky**
Studijní program: **Otevřené elektronické systémy**

II. ÚDAJE K BAKALÁŘSKÉ PRÁCI

Název bakalářské práce:

Charakterizace povrchů diamantových struktur

Název bakalářské práce anglicky:

Surface Characterization of Diamond Structures

Pokyny pro vypracování:

1. Study the principles and techniques of the atomic force microscopy.
2. Choose the suitable diamond structures and characterize their surfaces, especially the defects topography.
3. Analyze the characterization results with respect to the substrate orientation and boron doping level.

Seznam doporučené literatury:

- [1] Bert Voigtländer: Atomic Force Microscopy, Springer 2019
- [2] Shahram Soleymani et al.: Diamond nanocrystal thin films: Case study on surface texture and power spectral density properties, AIP Advances 10, 045206, 2020) <https://doi.org/10.1063/5.0003866>
- [3] SPM Principles [online], NT-MDT LLC, (c) 2022, [cit 2022-02-09] <https://www.ntmdt-si.com/resources/spm-principles>

Jméno a pracoviště vedoucí(ho) bakalářské práce:

doc. RNDr. Jan Voves, CSc. katedra mikroelektroniky FEL

Jméno a pracoviště druhé(ho) vedoucí(ho) nebo konzultanta(ky) bakalářské práce:

Datum zadání bakalářské práce: **10.02.2022**

Termín odevzdání bakalářské práce: **10.01.2023**

Platnost zadání bakalářské práce: **30.09.2023**

doc. RNDr. Jan Voves, CSc.
podpis vedoucí(ho) práce

doc. Ing. Stanislav Vítek, Ph.D.
podpis vedoucí(ho) ústavu/katedry

prof. Mgr. Petr Páta, Ph.D.
podpis děkana(ky)

III. PŘEVZETÍ ZADÁNÍ

Student bere na vědomí, že je povinen vypracovat bakalářskou práci samostatně, bez cizí pomoci, s výjimkou poskytnutých konzultací. Seznam použité literatury, jiných pramenů a jmen konzultantů je třeba uvést v bakalářské práci.

Datum převzetí zadání

Podpis studenta